Coupled-channel analysis of $K\Sigma$ production on the nucleon up to 2.0 GeV

Xu Cao,* V. Shklyar,† and H. Lenske‡

Institut für Theoretische Physik, Universität Giessen, D-35392 Giessen, Germany

A coupled-channel effective Lagrangian model respecting unitary and gauge invariance is applied to the combined analysis of $(\pi, \gamma)N \to K\Sigma$ reactions for center-of-mass energies up to 2 GeV. The recent photoproduction data obtained by the CLAS, CBELSA, LEPS, and GRAAL groups are included into our calculations with the aim to extract the resonance couplings to the $K\Sigma$ state. Both resonances and background contributions are found to be important to reproduce correct shapes of the angular distributions and polarization observables. Our description of the data is of good quality. The extracted properties of isospin $I = 3/2$ resonances are discussed in detail while the $I = 1/2$ resonances are largely determined by the nonstrangeness channels.

I. INTRODUCTION

Strangeness production on the nucleon has attracted a lot of attention over a long time. It is not only an elementary process of strangeness production, but also an ideal place to look for resonances that might be weakly coupled to the πN state. Recently, interest in the $K\Sigma$ channel has been revived by new photoproduction data with improved precision gained by several experimental groups, including LEPS [1–3], CLAS [4–9], CBELSA [10,11], GRAAL07 [12], and SAPHIR [13,14]. Strangeness electroproduction on the proton was also accurately measured by the CLAS [15] and A1 groups [16]. However, on theoretical side, most of the calculations [17–21] are based on the previous database, and the very recent data are not yet included in the analysis except for the Bonn-Gatchina partial wave analysis [22–27]. So it is meaningful to perform a full coupled-channel calculation based on the updated database combining both the πN and γN data. The Giessen K-matrix model is appropriate for this kind of analysis [28–32]. Results on nonstrangeness production in an updated version of the model have been published in a series of papers [33–36]. The partial wave amplitudes of $K\Lambda$ production and the coupling strengths of resonances to the $K\Lambda$ channel have also been extracted in Ref. [37]. Herein, we give a coherent coupled-channel analysis of the $K\Sigma$ production in the Giessen model.

Another motivation of the present paper is to resolve the current inconclusive status of different models on strangeness production, especially in the $K\Sigma$ channel. In the isobar model of Refs. [17,18], $K^0\Sigma^+$ photoproduction in addition to the $K^+\Sigma^0$ channel was found to be important for extracting knowledge on the background contributions. The $P_{13}(1720)$ resonance was shown to be essential to describe the data of this channel. In another isobar model [19] it was pointed out that the bare Born terms largely overestimated the data. In this calculation, five resonances, i.e., $S_{11}(1650)$, $P_{11}(1710)$, $P_{13}(1720)$, $S_{31}(1900)$, and $P_{31}(1910)$ were found

to be sufficient for achieving a good agreement with data. Only little or no evidence for a $D_{13}(1895)$ state was found, although that state seemed to emerge in the previous studies of the $K\Lambda$ photoproduction [38]. In Ref. [20], another very comprehensive isobar model was built for a combined analysis of photo- and electroproduction data. It included nucleonic resonances with spin up to $J = 5/2$, hyperonic resonances with spin $J = 1/2$, and kaonic resonances. A chiral quark model [21] with spin $J \leqslant 7/2$ resonances in the s channel showed that the contact term and the resonances with isospin $I = 3/2$, i.e., the $F_{37}(1950)$, $F_{35}(1905)$, $P_{33}(1920)$, and $P_{31}(1910)$, were dominant in the $K\Sigma$ photoproduction. After these very early isobar models, which were used to analyze the old data before 2002 (for data references, see [20,21]), a Regge-plus-resonance (RPR) model [39] was promoted to describe the new LEPS, CLAS, GRAAL, and SAPHIR data. Its background terms were deduced from the high-energy Regge-trajectory exchange in the t channel. Only four isospin $I = 1/2$ resonances, namely the $S_{11}(1650)$, $P_{11}(1710)$, $P_{13}(1720)$, and $P_{13}(1900)$, and four isospin $I = 3/2$ resonances, namely the $S_{31}(1900)$, $P_{31}(1910)$, $D_{33}(1700)$, and $P_{33}(1920)$, were needed to describe the data.

However, the coupled-channel analysis of the $K\Sigma$ photoproduction is, in fact, rather limited. The early Giessen model analysis [30–32] included resonances with spin up to $J = 3/2$ and obtained a fair agreement with the old $K\Lambda$ and $K\Sigma$ photoproduction data. A similar coupled-channel model with the K-matrix approach first developed by Usov and Scholten [40] and later extended by Shyam *et al.* [41] considered also resonances with spins up to $J = 3/2$ and fitted its parameters to the SAPHIR data [13,14]. Different gauge-restoration procedures were compared and the Davidson-Workman prescription, also being used in the Giessen model [31], was found to work best.

The Juelich group made a coupled-channel analysis of $\pi^+ p \to K^+\Sigma^+$ [42] which is a pure isospin $I = 3/2$ channel. The selection of final states was recently expanded to other $K\Sigma$ charged states, together with the ηN and $K\Lambda$ channels [43]. It was extended to πN photoproduction [44], but has not been employed to analyze strangeness photoproduction. A dynamical coupled-channel formalism developed by Juliá-Díaz *et al.* [45] used a chiral constituent quark model for

*xu.cao@theo.physik.uni-giessen.de

†vitaliy.shklyar@theo.physik.uni-giessen.de

‡horst.lenske@theo.physik.uni-giessen.de

strangeness photoproduction and investigated recent data on the $K\Lambda$ photoproduction combined with the $\pi^- p \to K\Lambda$ and $K^0\Sigma^0$ data. Including limited isospin $I = 3/2$ resonances, they found three new resonances: a D_{13}, a S_{11}, and a P_{13} with masses around 1954, 1806, and 1893 MeV, respectively. On the other hand it is not clear whether these resonances play a role in the $K\Sigma$ photoproduction. A chiral unitary framework addressing the importance of gauge invariance was developed in Ref. [46], but only focused on the close-to-threshold region of strangeness photoproduction due to the difficulty in dealing with the higher chiral orders.

Very recently the CLAS and CBELSA groups have released a lot of accurate data [8–11], enlarging considerably the database of strangeness production on the nucleon. Especially, the $\gamma p \to K^0\Sigma^+$ data published by the CBELSA group [10,11] are much more precise than the old SAPHIR data [14]. An interesting and important conclusion to be drawn from the CBELSA data is that most of the previous calculations overestimated the total cross section of this channel. While the two $\gamma p \to K^+\Sigma^0$ datasets published respectively by the CLAS [6] and SAPHIR collaborations [13] are not very consistent in the backward angles, the newly measured data by the CLAS group [8] agree well with the former CLAS data [6] and LEPS data [1–3]. In the Bonn-Gatchina isobar partial wave analysis of these data, the evidence for the $P_{13}(1900)$ resonance, which is not favored by diquark models, is reported [22–25], while the $P_{31}(1750)$ state found both in the Juelich [42] and Giessen coupled-channel models [30,31] plays no role. Keeping these problems in mind, we perform a new combined analysis by taking into account all new measurements from CLAS and CBELSA groups, etc.

We start in Sec. II with a brief outline of the main features of the Giessen model. The detailed calculations of $\pi N \to K\Sigma$ and $\gamma N \to K\Sigma$ and the extracted resonance parameters are presented in Sec. III. We finish with a short summary in Sec. IV.

II. GIESSEN MODEL

Though QCD has been established as a theory of the strong interaction for a long time, only effective degrees of freedom—mesons and baryons—are observed in experiment. Based on this observation, we develop a coupled-channel unitary Lagrangian model to study the reaction mechanism of the pion- and photoinduced reactions in the resonance region. The details of the interaction Lagrangians in the model and results for the nonstrange channels can be found in Refs. [30–32] and [33–36] respectively. Here, we only briefly outline the main ingredients of our model for simplicity. In order to obtain the scattering amplitude T_{fi}, the Bether-Salpeter equation is solved in the K-matrix approximation where the real part of the propagator G_{ab} is neglected:

$$T_{fi} = K_{fi} + i \sum_{a,b} K_{fa} \, \text{Im}(G_{ab}) T_{bi}, \qquad (1)$$

with i, f, and $a(b)$ being the initial, final, and intermediate states, respectively. The equation $K_{fi} = V_{fi} + \sum_{a,b} V_{fa} \text{Re}(G_{ab}) K_{bi}$ is reduced to $K = V$ in terms of the K-matrix approximation. In this way the solution of

the multichannel problem becomes feasible, satisfying the important condition of unitarity [30–32]. The validity of this approximation has been discussed in Refs. [22,30,33]. A proper theoretical definition of the resonance parameters would be to perform the calculation in the complex energy plane and search directly for the eigenstates of the underlying Hamiltonian, amounting to determination of the eigenvalues as poles on the second Riemann sheet. However, these kinds of calculations are numerically quite involved and are beyond the scope of our present work. Here we continue the previous efforts [28–37] to use the K-matrix approximation and quantify resonances by their input Breit-Wigner (BW) masses and widths. In the following text, the masses and widths quoted from the Particle Data Group (PDG) [47] are also the BW parameters.

After completing the partial-wave decomposition in terms of Wigner d functions, the Bether-Salpeter equation finally reduces to a set of algebraic equations for the scattering T matrix [32]:

$$T_{fi}^{J\pm,I} = \left[\frac{K^{J\pm,I}}{1 - iK^{J\pm,I}}\right]_{fi}, \qquad (2)$$

where $J^\pm,I$ are total spin, parity, and isospin of the final and initial states $f, i = \gamma N, \pi N, 2\pi N, \eta N, \omega N, K\Lambda$, and $K\Sigma$. The experimental observables, i.e., the cross sections and polarization observables, could be directly calculated by $T_{fi}^{J\pm,I}$, as explicitly expressed in Appendix G of Ref. [30] for pion-induced reactions and in Appendix E of Ref. [31] for photoinduced reactions. A graphical presentation of physical meaning and measurement of polarization observables can be found in Ref. [6]. In our model the 2π state is described in terms of the effective isovector-scalar meson. This allows us to control the $2\pi N$ inelastic flux and fix the resonance couplings to the $2\pi N$ channel [32].

The interaction potential (K matrix) is constructed as a sum of the s-, u-, and t-channel tree-level Feynman diagrams as depicted in Fig. 1. It is calculated from the corresponding effective interaction Lagrangians which respect chiral symmetry in the low-energy regime [30,31]. To cut off the contributions from large four-momenta $q^2 \gg \Lambda^2$, each meson and baryon vertex is dressed by a corresponding form factor of the form

$$F_p(q^2, m^2) = \frac{\Lambda^4}{\Lambda^4 + (q^2 - m^2)^2}. \qquad (3)$$

We use the same cutoffs for all resonances with given spin J, e.g., $\Lambda_i^{N^*(1535)} = \Lambda_j^{N^*(1650)}$ where indices i, j run over all final
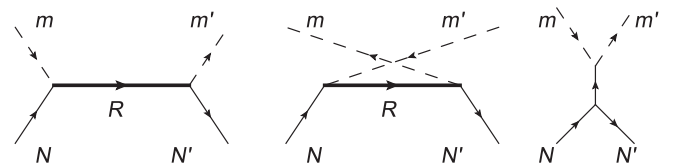

FIG. 1. s-, u-, and t-channel contributions to the interaction potential. The m and m' stand for initial and final mesons. The N, N', and R label initial, final, and intermediate baryons. Time flows from left to right.

TABLE I. Branching decay ratios $R_{K\Sigma} = \Gamma_{K\Sigma}/\Gamma_{\mathrm{tot}}$ of $I = 1/2$ resonances into the $K\Sigma$ final state extracted in the present calculation. In parentheses, the sign of corresponding coupling constant is shown (all πN couplings are chosen to be positive; see [33]). The BW masses and total widths are given in MeV and the decay ratios $R_{K\Sigma}$ in percent.

N^*	BW mass[a]	Γ_{tot}[a]	$R_{K\Sigma}$	$R_{K\Sigma}$[b]	Rank
$S_{11}(1535)$	1526	135	-0.64[c]	0.83[c]	**
$S_{11}(1650)$	1664	119	-0.81[c]	-0.59[c]	***
$P_{11}(1440)$	1517	608	-0.45[c]	0.53[c]	***
$P_{11}(1710)$	1723	403	$0.1(-)$	$12.6(-)$	*
$P_{13}(1720)$	1700	154	$0.0(-)$	$0.0(-)$	**
$P_{13}(1900)$	1998	401	$0.4(+)$	$2.0(-)$	**
$D_{13}(1520)$	1505	103	1.35[c]	1.13[c]	***
$D_{13}(1950)$	1935	858	$0.0(-)$	$0.3(+)$	*
$D_{15}(1675)$	1665	147	$5.4(+)$		***
$F_{15}(1680)$	1676	112	$65.9(-)$		**
$F_{15}(2000)$	1946	197	$0.0(+)$		**

[a]Fixed in the previous calculations [33–35].
[b]The C-p-$\gamma+$ results from a previous Giessen model analysis [30].
[c]The coupling is given since the resonance BW mass is below the threshold.

states. We also choose the cutoff at the $NK\Sigma$ vertex with the same value of the nucleon cutoff: $\Lambda_{NK\Sigma} = \Lambda_N = 0.95$ GeV. Hence, the number of free parameters is largely decreased.

The nonresonant part of the transition amplitude of $(\pi, \gamma)N \to K\Sigma$ is the same as that used in the previous Giessen model studies [30,31,37]. It consists of the nucleon Born term and t-channel contributions with the K^*, K_0^*, and K_1 mesons in the intermediate state. It should be mentioned that t-channel K_1 meson exchange only contributes to $\gamma N \to$

$K\Sigma$, and K_0^* meson exchange only to $\pi N \to K\Sigma$. The K^* meson exchange contributes to both reactions. The couplings $g_{K^*K\pi}$, $g_{K_0^*K\pi}$, $g_{K^*K\gamma}$, and $g_{K_1K\gamma}$ are calculated from the experimental decay widths of the PDG compilation [47]; see [31] for the values. We use the same $\Lambda_t = 0.77$ GeV at the corresponding t-channel vertices for both associated strangeness and nonstrangeness channels [37]. Similar to our previous studies [30,31] we do not consider the u-channel diagrams to the $(\pi, \gamma)N \to K\Sigma$ reaction in order to keep the model as simple as possible. The calculation of such diagrams would require *a priori* unknown couplings to the intermediate strange baryons, i.e., the Λ^* and Σ^* resonances.

We treat the photoproduction reactions perturbatively owing to the smallness of the electromagnetic coupling. This means that the summation on intermediate states runs only over hadronic states by neglecting the γN state in Eq. (2). This prescription has been checked in [31] and found to be very accurate.

III. NUMERICAL RESULTS AND DISCUSSION

In our calculation we include 11 isospin $I = 1/2$ resonances and 9 isospin $I = 3/2$ resonances, listed in Tables I and II, respectively. The effects of isospin $I = 1/2$ resonances have been extensively studied in the production of ωN [34], ηN [35,36], and $K\Lambda$ [37] by including spin $J \leqslant 5/2$ resonances [33]. High spin resonances are found to be important in the ωN production [34]. A discussion of the $I = 1/2$ partial waves in elastic $\pi N \to \pi N$, the proton and neutron multipoles of $\gamma N \to \pi N$, the $\pi N \to 2\pi N$ total partial wave cross sections, and the πN inelasticity can be found in Ref. [34]. In this paper we continue the investigations of the $I = 1/2$ and $3/2$ sectors with the parameters fitted to newly published $K\Sigma$ photoproduction data together with

TABLE II. The first and second lines are the properties of $I = 3/2$ resonances extracted in the present calculations and the C-p-$\gamma+$ results from a previous Giessen model analysis [30], respectively. The BW masses and total widths are given in MeV and the decay ratios $R_{ab} = \Gamma_{ab}/\Gamma_{\mathrm{tot}}$ in percent. The electromagnetic helicity amplitudes $A_{\frac{1}{2}}$ and $A_{\frac{3}{2}}$ are in units of 10^{-3} GeV$^{-1/2}$.

Δ^*	BW mass	Γ_{tot}	$R_{\pi N}$	$R_{2\pi N}$	$R_{K\Sigma}$	$A_{\frac{1}{2}}$	$A_{\frac{3}{2}}$	Rank
$S_{31}(1620)$	1598	209	26.8	$73.2(+)$	-0.35[a]	-58		**
	1611	196	34.3	$65.7(-)$	0.14[a]	-50		
$P_{31}(1750)$	1773	651	1.6	$97.5(+)$	$0.9(+)$	1		***
	1712	660	0.8	$99.1(+)$	$0.1(+)$	53		
$P_{33}(1232)$	1227	110	100.0	$0.0(-)$	0.00[a]	-128	-253	**
	1228	106	100.0	$0.21(-)$[b]	0.00[a]	-128	-247	
$P_{33}(1600)$	1694	515	14.9	$85.1(+)$	-0.10[a]	-10	-17	***
	1667	407	13.3	$86.7(+)$	0.03[a]	0	-24	
$P_{33}(1920)$	2069	767	4.1	$95.1(-)$	$0.7(-)$	21	25	**
	2057	494	15.9	$81.6(-)$	$2.4(-)$	-7	-1	
$D_{33}(1700)$	1673	766	15.0	$85.0(+)$	0.17[a]	97	147	***
	1678	591	13.9	$86.1(+)$	0.75[a]	96	154	
$D_{35}(1930)$	2001	440	7.2	$78.8(+)$	$14.1(+)$	-66	1	***
$F_{35}(1905)$	1842	619	6.5	$93.4(-)$	$0.003(-)$[b]	54	-127	***
$F_{35}(2000)$	2160	313	1.5	$98.5(-)$	$0.89(-)$[b]	18	-23	*

[a]The coupling is given since the resonance BW mass is below the threshold.
[b]Decay ratio in 0.01%.

TABLE III. Born couplings in the present calculations (first line) compared to the previous Giessen model (second line) [30].

$g_{NK\Sigma}$	$g_{NK_0^*\Sigma}$	$g_{NK^*\Sigma}$	$\kappa_{NK^*\Sigma}$	$g_{NK_1\Sigma}$	$\kappa_{NK_1\Sigma}$
−5.41	−32.94	0.83	−1.71	3.67	−2.58
2.48	−26.15	4.33	−0.86	22.80	2.40

the previous $\pi N \to K\Sigma$ measurements (for data references, see, e.g., [30,31]) in the energy region $\sqrt{s} \leqslant 2.0$ GeV. The included $K\Sigma$ photoproduction data are those of $\gamma p \to K^+\Sigma^0$ published by the LEPS [1–3], CLAS [6,8], and GRAAL [12] groups, and those of $\gamma p \to K^0\Sigma^+$ released by the CLAS [4] and CBELSA [10] collaborations. The SAPHIR data have been left out here because of the already mentioned inconsistencies of the $K^+\Sigma^0$ data [13] with the corresponding CLAS and GRAAL data (for the details, see Ref. [8]). Also, the $K^0\Sigma^+$ SAPHIR data [14] have much bigger error bars than those of the CBELSA and CLAS groups. Here, the data before 2002 are also no longer used. The Giessen model results for these old data can be found in our previous publications [30,31].

In the present calculation we achieve a quite satisfactory description of the $\gamma p \to K^+\Sigma^0$ data ($\chi^2 = 1.8$) and the $\gamma p \to K^0\Sigma^+$ data ($\chi^2 = 2.0$). However, the pion-induced strangeness production reactions are described with slightly worse quality as indicated by the corresponding χ^2 values of $\chi^2 = 4.1, 3.2$, and 2.8 for the $\pi^+ p \to K^+\Sigma^+, \pi^- p \to K^0\Sigma^0$, and $\pi^- p \to K^+\Sigma^-$ reactions, respectively. The parameters that have been varied in our fit simultaneously to the $I = 1/2$ and 3/2 sectors are shown in Tables I–III. Due to the smallness of the $N^*K\Sigma$ couplings, all previously obtained BW masses, branching ratios, and couplings corresponding to nonstrangeness production [34] are hardly affected by the additional $K\Sigma$ photoproduction data, so in the following subsection we will concentrate on the properties of the $I = 3/2$ resonances.

A. Partial wave analysis in the isospin 3/2 sector

The parameters of the isospin $I = 3/2$ resonances used in our calculations were extensively discussed in the previous publications [30,31,33]. Here we will comment on the new features after adding resonances with spin $J = 5/2$ and updating our database. The calculated isospin $I = 3/2$ partial waves of $\pi N \to \pi N$, $\pi N \to 2\pi N$, and multipoles of $\gamma N \to \pi N$ are shown in Figs. 2, 3, and 4, respectively. In the following we compare our parameters of $I = 3/2$ resonances with those of other coupled-channel models, i.e., the previous Giessen model [30,31], the Usov and Scholten model [40,41], and the Juelich model [42], and those of partial wave analyses, i.e., the Bonn-Gatchina [22–27], the KSU [48,49], the Pitt-ANL [50], and the GWU [51–55] models.

S_{31} *partial wave.* The first S_{31} resonance with mass around 1620 MeV is well identified in many analyses due to the obvious structures of S_{31} partial waves of the $\pi N \to \pi N$ and $\pi N \to 2\pi N$, and also the unambiguous $E_{0+}^{3/2}$ multipole in this energy region [54,55]. Our present fit of this multipole is much better than that in the old Giessen calculations
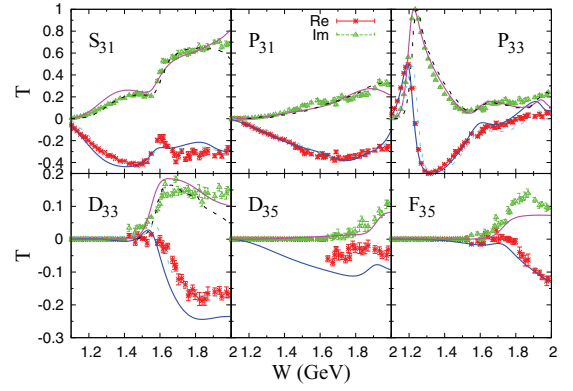

FIG. 2. (Color online) The elastic πN partial waves for $I = 3/2$. The upper solid (magenta) lines, dashed (dark grey) lines, and triangle (green) points are the imaginary parts of the amplitude of our model, the previous Giessen model [30], and the GWU/SAID analysis [52], respectively. The lower solid (blue) lines, dashed (cyan) lines, and star (red) points are the corresponding real parts of the amplitude.

where an obvious deviation between theory and data appears between 1.4 and 1.6 GeV [30]; see Fig. 4. However, the description of this elastic πN partial wave become worse as shown in Fig. 2, which indicates that the model faces a demanding challenge from the new $K\Sigma$ photoproduction data. The S_{31}-wave inelasticity mainly comes from $2\pi N$ channel as can be seen from Fig. 3.

The second S_{31} resonance around 1900 MeV is controversial and only of two-star status in PDG ranking [47]. It is found in the partial wave analyses of KSU [48,49] and Pitt-ANL [50] but not confirmed by the GWU survey [51,52]. The Bonn-Gatchina group previously concluded that it did
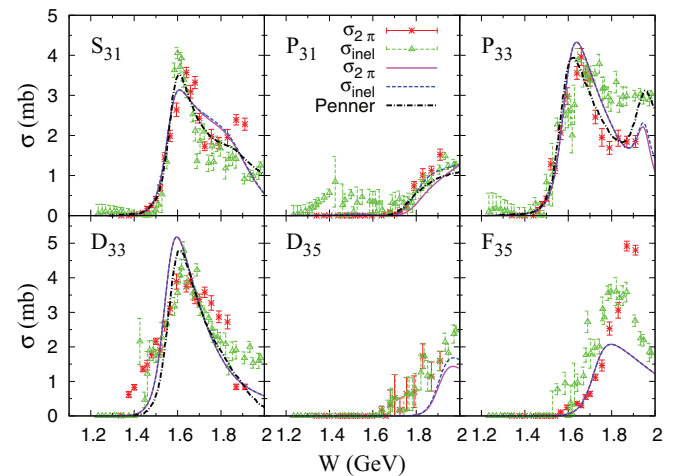

FIG. 3. (Color online) The inelastic $2\pi N$ total partial wave cross sections for $I = 3/2$. The solid lines (magenta) and dashed lines (blue) are the calculated cross section and inelasticity, respectively. The dash-dotted (dark grey) lines are the calculated cross sections of the previous Giessen model [30]. The triangle points (green) and star points (red) are the total cross section and inelasticity from Manley *et al.* [53] and the GWU group [52], respectively. In S_{31}, D_{33}, and F_{35} waves, the calculated inelasticities almost coincide with the calculated $2\pi N$ cross sections.
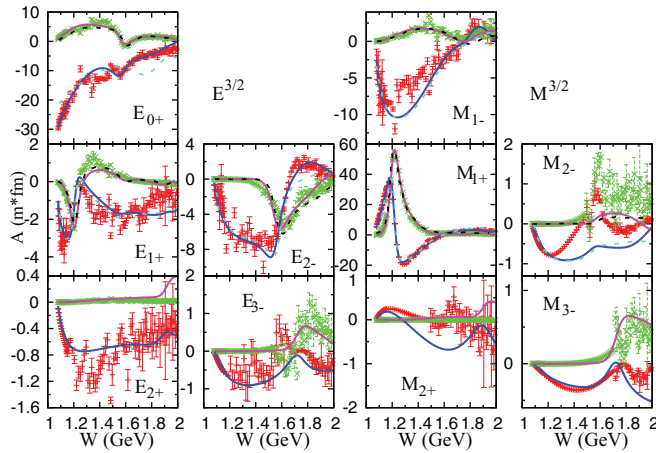
FIG. 4. (Color online) The $\gamma N \to \pi N$ multipoles for $I = 3/2$. The upper solid (magenta) lines, dashed (dark grey) lines and triangle (green) points are imaginary parts of amplitude of our model, the previous Giessen model [30], and the GWU analysis [54], respectively. The lower solid (blue) lines, dashed (cyan) lines, and star (red) points are the corresponding real parts of amplitude.

not need to include this resonance [24–26]. However, they do add it to their recent analysis [22,23] and find that its properties are consistent with those obtained in the recent KSU analysis [49]. In the previous Giessen calculations, the $S_{31}(1900)$ emerges only in the Pascalutsa prescription of the $J = 3/2$ resonances vertices [30,31], but the evidence is weak and of rather nonresonant nature. In our present calculations we reinvestigated the relevance of this resonance and find a small electromagnetic helicity amplitude $A_{1/2}$ with a value around -10×10^{-3} GeV$^{-1/2}$. In the region close to 2 GeV, this $S_{31}(1900)$ creates small structures in the S_{31} waves of πN elastic and $2\pi N$ channels and in the $E_{0+}^{3/2}$ multipole of πN photoproduction, which are still within the experimental uncertainties. But for $K\Sigma$ production it is irrelevant, being totally immersed into the background. The contribution to the cross section of that state can be fully compensated by a small variation of the Born couplings. So we do not include this second S_{31} resonance here. Other coupled-channel models, i.e., those of Juelich and of Usov and Scholten include only $S_{31}(1620)$, too. Our extracted BW mass and width of $S_{31}(1620)$ are respectively 1598 and 209 MeV, which are close to the values of the recent KSU analysis [49].

P_{31} *partial wave.* In our model only one $P_{31}(1750)$ is sufficient to reproduce a correct shape in the partial waves of πN and $2\pi N$ channels, though its electromagnetic properties have large uncertainty because of the big error bars in the $M_{1-}^{3/2}$ multipoles [54,55] as can be seen in Fig. 4. Figure 3 shows that the P_{31} inelasticity comes mainly from $2\pi N$ channel but also from the $K\Sigma$ final state with the branching ratio Br$(P_{31}(1750) \to K\Sigma) \simeq 0.90\%$ as shown in Table II. The Pitt-ANL [50] and old KSU models [48] include the additional $P_{31}(1910)$ resonance and find a $P_{31}(1750)$ with the mass at about 1730 MeV, which is a little lower than ours. The GWU analysis [51,52] finds a P_{31} pole around 1770 MeV but attributes it to the $P_{31}(1910)$ resonance due to its large mass, which is above 2000 MeV and much higher than the value

in other models. In the Juelich approach [42] the $P_{31}(1750)$ state is dynamically generated and the $P_{31}(1910)$ state is a genuine resonance. The recent KSU [49] and Bonn-Gatchina [22] models also found only the $P_{31}(1910)$ resonance but no evidence for the $P_{31}(1750)$ state. The Usov and Scholten calculation [40,41] does not include any P_{31} resonance.

P_{33} *partial wave.* In our analysis, we need three resonances in this partial wave: $P_{33}(1232)$, $P_{33}(1600)$, and $P_{33}(1920)$. This selection of states is widely confirmed by different groups, i.e., Pitt-ANL, KSU, and Bonn-Gatchina. Especially the properties of $P_{33}(1232)$ are well established because of the accurate $E_{1+}^{3/2}$ and $M_{1+}^{3/2}$ multipole data at this energy, as shown in Fig. 4. A $P_{33}(1920)$ whose BW mass is found to be above 2 GeV is needed to deliver additional πN strength in this partial wave at high energies. But in the GWU model only the first two P_{33} resonances are included into the previous fit [51], and their recent calculation takes only the first resonance into account [52]. In the Juelich model [42] the $P_{33}(1600)$ state is a dynamically generated state, while the other two P_{33} states are of genuine character. The $P_{33}(1600)$ is not present in the analysis of Usov and Scholten [40,41] but the other two states, the $P_{33}(1232)$ and $P_{33}(1920)$, are included into their model. Here it is worth mentioning that the $P_{33}(1600)$ is found to be important in the double-pion production in nucleon-nucleon collisions, especially in the $pp \to nn\pi^+\pi^+$ channel where only isospin $I = 3/2$ resonances can contribute [56]. The authors of Ref. [56] obtain 350 MeV for the BW width of $P_{33}(1600)$.

In fact, as seen in Fig. 2 there is no clear resonance structure in the elastic πN partial wave at high energies, so it is a little difficult to establish the existence of $P_{33}(1600)$ and $P_{33}(1920)$ unambiguously. For these two higher lying P_{33} states, we find small electromagnetic contributions as shown in Table II, so they have hardly any visible structure in the $M_{1+}^{3/2}$ and $E_{1+}^{3/2}$ multipoles. Also, the large error bars in the $E_{1+}^{3/2}$ multipole at high energies inhibit a solid conclusion.

As already addressed in previous Giessen model analyses [30], the $2\pi N$ channel is dominant in the P_{33}-wave inelasticity but the observed inelastic partial-wave cross section is higher than our model calculation by about 1 mb above 1.7 GeV, as can be clearly seen in Fig. 3. As a result, we still miss inelastic contributions of about 1 mb in the P_{33} partial wave at high energies in the present model, similar to the case in the P_{13} wave [30]. This is a possible hint for the contribution of a $3\pi N$ state such as $\rho\Delta$.

D_{33} *partial wave.* In this partial wave we find only the $D_{33}(1700)$ resonance and, in this respect, agree with other models except the old KSU analysis [48] where a second $D_{33}(1940)$ was found. However, the recent KSU investigation [48] does not find this $D_{33}(1940)$ resonance so it seems that now all analyses are converging to only one D_{33} state. The D_{33} wave in the πN elastic channel shows a distinct resonance structure as can be seen in Fig. 2, so the BW mass of $D_{33}(1700)$ is fixed with good accuracy. The agreement between the calculated real part of the D_{33} partial wave and the GWU single-energy elastic πN solution [54,55] becomes a little worse after the inclusion of the new $K\Sigma$ photoproduction data, as shown in Fig. 2.

As in the previous Giessen model investigation [30], the calculated $2\pi N$ inelasticity does not follow well the results of Manley *et al.* [53] below the $D_{33}(1700)$ resonance position, as shown in Fig. 3. As discussed in the case of the P_{33} wave, this would be amended by an extension of the model into the $3\pi N$ sector.

In our previous studies [31], there were also discrepancies in the description of the $M_{2-}^{3/2}$ multipole, and it is difficult to extract accurate helicity amplitudes there. It was supposed that this was due to the lack of background contribution in this multipole. The present results demonstrate a better agreement for the imaginary part but the strength of the real part is still not big enough to explain the data, as depicted in Fig. 4. The trend of the $E_{2-}^{3/2}$ multipole is nicely reproduced, though small deviations are seen at the intermediate energies.

D_{35} partial wave. In this channel we include the $D_{35}(1930)$ resonance. Our present calculations have a problem in the description of this amplitude, as seen in Fig. 2. In the previous fit to only pion-induced reactions we have found that it is difficult to get a reasonable agreement with the GWU results for this partial wave if only $D_{35}(1930)$ state is taken into account [33]. Being extended into the photoinduced reactions, our model demonstrates a better result for the imaginary part of the D_{35} wave than the situation for the purely hadronic results, as can be seen from Fig. 2. It is interesting to note that similar problems are experienced in the Juelich model [42]. In addition, the calculated $2\pi N$ cross section tends to be below the results of Manley *et al.* [53] as shown in Fig. 3, which might point out some deficiency in the description of the $2\pi N$ channel.

In Fig. 4 some deviations from the GWU analysis can be seen in the real part of the $M_{2+}^{3/2}$ amplitude, but there are large error bars in this multipoles of the GWU analysis [54,55]. The background constitutes the main contribution to the $M_{2+}^{3/2}$ and $E_{2+}^{3/2}$ multipoles and the $D_{35}(1930)$ resonance has small structures at high energies due to its small electromagnetic couplings.

Other models also include this $D_{35}(1930)$ with the only exception of the Bonn-Gatchina model which does not consider any D_{35} resonance. A second $D_{35}(2350)$ is included in the Pitt-ANL and the old GWU calculations, but recent GWU analyses find no indication for this resonance. In our model we do not consider this high mass state because of its minor contribution to the energy region below 2 GeV.

F_{35} partial wave. In our previous hadronic result it was sufficient to take a single $F_{35}(1905)$ resonance into account for a good description of this partial wave [33]. In the present analysis, the imaginary part of amplitude of the elastic πN channel in Fig. 2 and the partial wave cross section of the $2\pi N$ channel in Fig. 3 obviously are both underestimated above 1.8 GeV, so other inelastic channels such as $3\pi N$ may also contribute. The $F_{35}(1905)$ state contributes also to the $E_{3-}^{3/2}$ and $M_{3-}^{3/2}$ multipoles, as can be seen in Fig. 4. But here we include another $F_{35}(2000)$ resonance, though its BW mass is close to the upper energy limit of our calculation. The reason is that it considerably improves the high energy tail of our S_{31}, P_{31}, and P_{33} partial waves in the elastic πN channels. However, the signal of this state is hard to resolve unam-

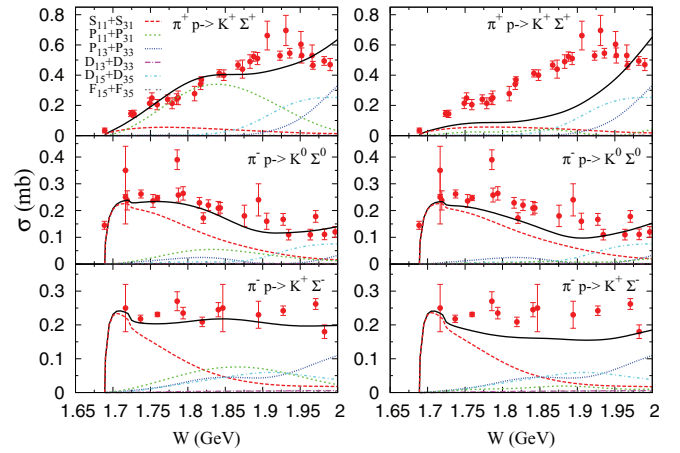FIG. 5. (Color online) The total cross sections of $\pi N \to K\Sigma$. Left panel: the full model calculation. Right panel: the model calculation with $P_{31}(1750)$ turned off. The solid (black), dashed (red), short-dashed (green), dotted (blue), dot-dashed (magenta), dot-short-dashed (cyan), and double-short-dashed (grey) lines correspond to the full results, the S_{11} ($\frac{1}{2}^-$), P_{11} ($\frac{1}{2}^+$), P_{13} ($\frac{3}{2}^+$), D_{13} ($\frac{3}{2}^-$), D_{15} ($\frac{5}{2}^-$), and F_{15} ($\frac{5}{2}^+$), respectively.

biguously because of its small partial decay width to the πN channel.

The existence of $F_{35}(1905)$ is confirmed by many other studies because of its obvious role in the F_{35} wave of the πN elastic scattering. Another F_{35} resonance with a lower mass of about 1750 MeV found in the old KSU study [48] is not needed in our calculations. The ambiguity of $F_{35}(2000)$ is still unresolved. Though the latest GWU [52], Bonn-Gatchina [22,23] analyses as well as many other former analyses find no evidence for this resonance; the recent KSU survey [49] finds it with mass and width of 2015(24) and 500(52) MeV, respectively, which has to be compared to our values of 2160 and 313 MeV, listed in Table II.

B. Results for the $\pi N \to K\Sigma$ reaction

Our calculated total cross sections are compared to the available data in Fig. 5. As can be seen, when both isospin $I = 1/2$ and $I = 3/2$ channels are accessible, the S_{11} wave dominates at threshold. Other partial waves, namely P_{31}, P_{33}, D_{35}, and D_{15}, contribute at high energies. The effect from D_{13} and D_{33} waves is hardly seen. When only isospin $I = 3/2$ is allowed, i.e., the $\pi^+ p \to K^+\Sigma^+$ channel, the P_{31} wave dominates at threshold and the D_{35} and P_{33} waves become important at high energies. At the region very close to threshold, the contribution of the S_{31} wave is noticeable. The F_{15} and F_{35} partial waves tend to be negligible in whole energy range.

The nonresonant part of the amplitude in the $\pi^- p \to K^+\Sigma^-$ reaction is negligibly small but it is seen in the $\pi^- p \to K^0\Sigma^0$ and $\pi^+ p \to K^+\Sigma^+$ channels. This is because the contribution from the nucleon Born term is very small and the nonresonant contribution comes mainly from the t-channel K_0^* meson exchange. In our results the coupling constant of $NK^*\Sigma$ is much smaller than that in our previous

investigations; see Table III. As a result, the contribution from the t-channel K^* meson exchange is reduced. Though effects of the nonresonant part of the amplitude affect the Σ polarization, its overall contribution is very small.

It should be stressed that the exact shapes of angular distributions and polarization observables are produced by the interference of several partial waves. So sometimes even contributions of small magnitude will influence a shape significantly. Therefore it is necessary to look deeper into the reaction amplitudes, including also the weakly populated reaction channels. In the following two subsections we concentrate on the differential cross sections and polarization observables of the $\pi^+ p \to K^+\Sigma^+$ and $\pi^- p \to K^+\Sigma^-/K^0\Sigma^0$ reactions, respectively.

1. Results for the $\pi^+ p \to K^+\Sigma^+$ reaction

The $\pi^+ p \to K^+\Sigma^+$ channel is purely isospin $I = 3/2$. Our conclusion on this channel is similar to the previous Giessen model study. In the region very close to threshold, the S_{31} wave is dominated by the $S_{31}(1620)$ resonance whereas the S_{11}-wave contribution is forbidden. In the considered energy region, our present calculations show that the shape of the $\pi^+ p \to K^+\Sigma^+$ angular distributions is dominated by the $P_{31}(1750)$ resonance together with the $P_{33}(1600)$, $D_{33}(1700)$, and $D_{35}(1930)$ states, especially enhancing the strength of a broad peak at the backward angles, as shown in Fig. 6. For the Σ polarization in Fig. 7, the $P_{31}(1750)$ resonance is important at all energies and the $D_{33}(1700)$ is essential already close to threshold. It should be mentioned that the $D_{35}(1930)$ is responsible for the dip at forward angles above 1.8 GeV in the angular distribution (see Fig. 6) and the steep rise at intermediate angles seen in the Σ polarization (see Fig. 7). It seems that this result resolves the apparent confusion in the D_{35} wave of elastic πN collisions mentioned in Sec. III A: the $D_{35}(1930)$ resonance is definitely
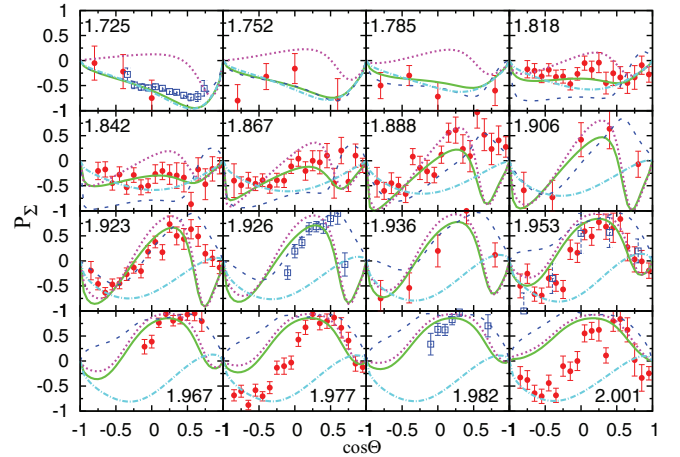
FIG. 7. (Color online) The Σ polarization of $\pi^+ p \to K^+\Sigma^+$ reaction. The meaning of the lines is the same as in Fig. 6. The numeric values label the center-of-mass energies in units of GeV.

needed for a good description of the $\pi^+ p \to K^+\Sigma^+$ data. Similar to the other two charged channels, the transition current flows from $P_{31}(1750)$ into the D_{35} and P_{33} partial waves at high energies. As a result, these two partial waves exceed other partial wave contributions to be the strongest above 1.95 GeV, inducing a steep rise of the total cross section in Fig. 5. In Figs. 6 and 7, we also show results of calculations where the $P_{31}(1750)$ resonance was turned off. The effect from $F_{35}(1905)$ and $F_{35}(2000)$ can be seen in the angular distributions and Σ polarizations though the overall contribution from these states is found to be small.

However, the conclusions vary much in different models. In the Juelich model [42], the $\pi^+ p \to K^+\Sigma^+$ reaction is dominated by the $S_{31}(1620)$, while the P_{33} wave dominated by the $P_{33}(1600)$ and $P_{33}(1920)$ resonances ranks second but is much weaker than the contribution of the $S_{31}(1620)$ state. At energies around 2.0 GeV, the $F_{37}(1950)$ begins to exceed the P_{33} contribution but still is smaller than the S_{31} wave. In the Bonn-Gatchina analysis of this reaction [23], $P_{33}(1920)$ is identified to be the most essential, and the interference of $J = 7/2^+$ and $J = 5/2^+$ channels plays an important role at high energies. So it seems that the $K^+\Sigma^+$ production mechanism needs further clarification. Juliá-Díaz *et al.* [45] achieve a reasonable agreement with the $\pi^- p \to K^0\Sigma^0$ data by including only three isospin $I = 3/2$ resonances $S_{31}(1900)$, $P_{31}(1910)$, and $S_{33}(1920)$ together with several isospin $I = 1/2$ resonances.

2. Results for the $\pi^- p \to K^+\Sigma^-$ and $K^0\Sigma^0$ reactions

In the $\pi^- p \to K^+\Sigma^-$ and $K^0\Sigma^0$ channels, from threshold up to 1.8 GeV, the $S_{11}(1650)$ resonance dominates the energies, and its destructive interference with the $S_{11}(1535)$ is also important. Close to threshold the effect from the $S_{31}(1620)$ resonance is seen but is much smaller than that of the $S_{11}(1650)$ state. The small kink at around 1.72 GeV is caused by the ωN threshold effect. At higher energies, the contributions of $P_{31}(1750)$, $P_{11}(1440)$, $P_{33}(1600)$, and $D_{35}(1930)$ become
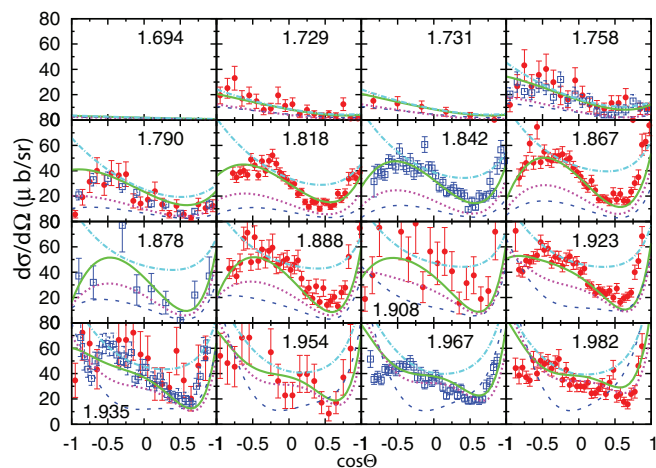

FIG. 6. (Color online) The differential cross section of the $\pi^+ p \to K^+\Sigma^+$ reaction. The solid (green), dashed (blue), dotted (magenta), and dash-dotted (cyan) lines are the full model calculation and the model calculations with $P_{31}(1750)$, $D_{33}(1700)$, and $D_{35}(1930)$ turned off, respectively. The numeric values label the center-of-mass energies in units of GeV.
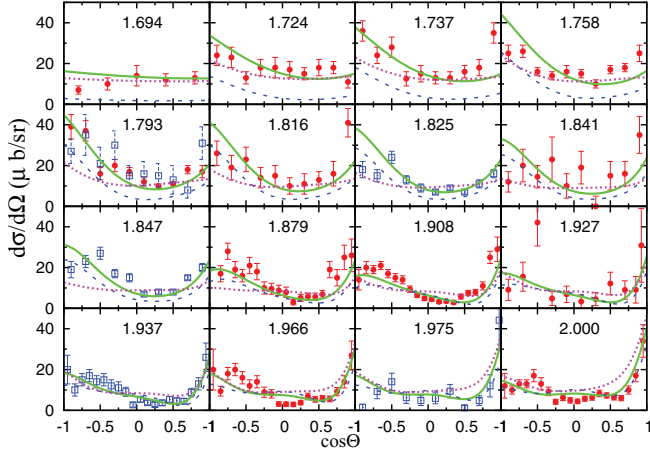
FIG. 8. (Color online) The differential cross section of the $\pi^- p \to K^0 \Sigma^0$ reaction. The solid (green), dashed (blue), and dotted (magenta) lines are the full model calculation and the model calculations with $S_{11}(1650)$ and $F_{15}(1680)$ turned off, respectively. The numeric values label the center-of-mass energies in units of GeV.

FIG. 10. (Color online) The differential cross section of the $\pi^- p \to K^+ \Sigma^-$ reaction. The solid (green), dashed (blue), dotted (magenta), and dash-dotted (cyan) lines are the full model calculation and the model calculations with $S_{11}(1650)$, $D_{15}(1675)$, and $F_{15}(1680)$ turned off, respectively. The numeric values label the center-of-mass energies in units of GeV.

comparable. The important role of $D_{33}(1700)$ and $D_{15}(1675)$ states is clearly visible in angular distributions of various observables over the whole considered energy region, though they are small in the total cross sections. Such a behavior indicates that the enhancement is due to interference effects which obviously are removed in the total cross sections by the angular integration. The D_{35} and P_{33} waves which mainly originate from $D_{35}(1930)$ become significant in the energy tail while the contribution of $P_{31}(1750)$ decreases steadily. Our results are different from our previous investigation [30], where the $S_{11}(1650)$ resonance dominates in the close-to-threshold region but $P_{11}(1710)$ and $P_{31}(1750)$ are the strongest contributions for increasing energies. As we have pointed out, the impact from the $J = 5/2$ resonances, which were not included in the previous Giessen model [30], is visible. In Figs. 8–10, we compare our full results to the calculations
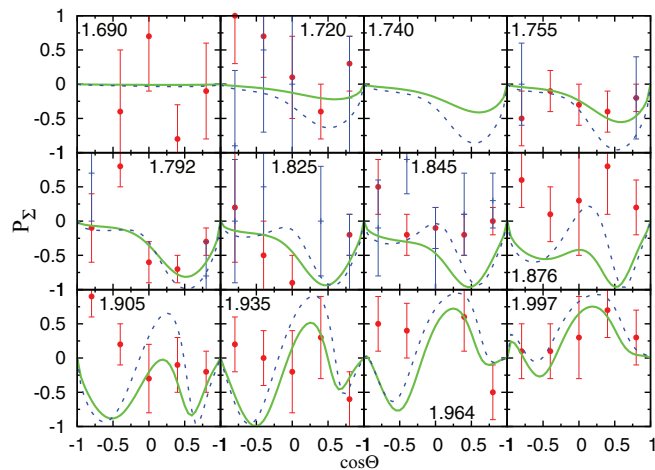
where the $S_{11}(1650)$ resonance was turned off in order to illustrate the role of this resonance.

In the $\pi^- p \to K^+ \Sigma^-$ and $\pi^- p \to K^0 \Sigma^0$ reactions, the contribution of the $P_{31}(1750)$ resonance is suppressed and it is only seen in the Σ polarization of the $\pi^- p \to K^0 \Sigma^0$ channel. Instead, $S_{11}(1650)$, $P_{33}(1600)$, $D_{15}(1675)$, $D_{35}(1930)$, and $F_{15}(1680)$ all together determine the shape of the angular distributions and Σ polarizations of these two reactions. The $D_{15}(1675)$ state is responsible for the steep forward rise in angular distributions of the $\pi^- p \to K^+ \Sigma^-$ reaction at intermediate energies, as seen in Fig. 10. The $F_{15}(1680)$ is significant in the backward structures in the angular distributions of both channels, as respectively shown in Fig. 8 and Fig. 10. The contribution of the $F_{15}(2000)$ resonance is very small but still noticeable.

C. Results for the $\gamma p \to K \Sigma$ reaction

As depicted in the lower panels of Fig. 11, the total cross section of the $\gamma p \to K^+ \Sigma^0$ reaction is largely dominated by the S_{I1} channel while the contribution from other partial waves is small. In the case of the $\gamma p \to K^0 \Sigma^+$ channel the situation is much more complicated. The S_{I1}, P_{I1}, and P_{I3} partial wave amplitudes are the most important ones. The S_{I1} component has a second maximum around 1.93 GeV which is induced by the interference between the resonances and background generated by t- and u-channel interactions. However, in the finally obtained scattering amplitudes the two types of dynamical contributions are mixed by solving Eq. (1) for the scattering T matrix. We do not attempt or even need to decompose artificially the derived T-matrix elements or cross sections into background and resonance components, but only state, where meaningful, the net result. In all of the calculations, coupled-channels effects are extremely important. The large contributions of higher-order terms due

FIG. 9. (Color online) The Σ polarization of $\pi^- p \to K^0 \Sigma^0$ reaction. The meaning of the lines is the same as in Fig. 8. The numeric values label the center-of-mass energies in units of GeV.
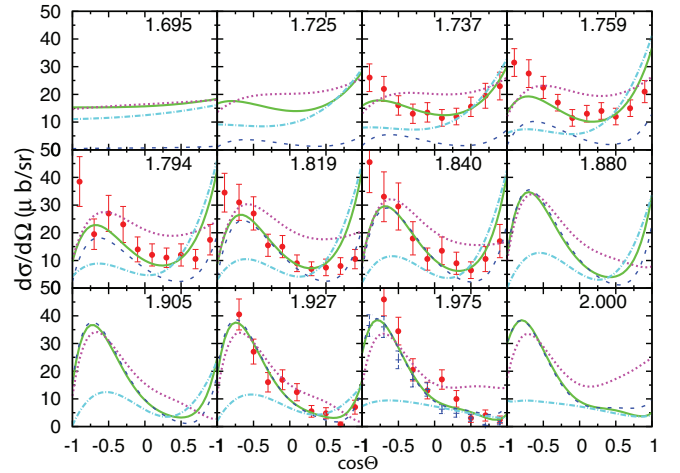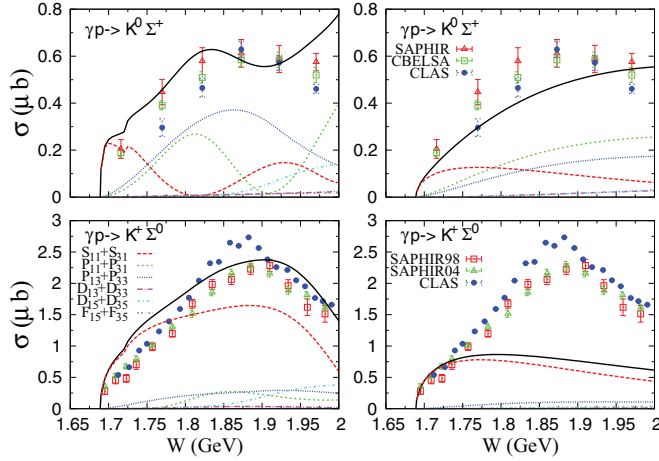
FIG. 11. (Color online) The total cross sections of $\gamma N \to K\Sigma$. Left panel: the full model calculation. Right panel: the Born terms and t-channel meson exchange only. The line types are the same as in Fig. 5. The data are taken from SAPHIR [13,14], CBELSA [10], and CLAS [4,6]. The SAPHIR data is only for comparison and is not used in the parameters' fitting.

FIG. 12. (Color online) The differential cross section of $\gamma p \to K^+\Sigma^0$ reaction. The solid (green), dashed (blue), dotted (magenta), and dash-dotted (cyan) lines are the full model calculation, the contribution of the Born terms, and the model calculations with $S_{11}(1650)$ and $S_{31}(1620)$ turned off, respectively. The data are taken from CLAS [8]. The numeric values label the center-of-mass energies in units of GeV.

to the repeated interactions in the summation of the scattering series can be seen quantitatively in various figures where the input Born terms are compared to the final result of the full T-matrix solution. The P_{I1} partial wave cross section rises steeply, exceeding the contribution of other partial waves in the region from 1.8 to 1.95 GeV and is responsible for the steep rise of the total cross section at high energies.

It is known that the Born term is enhanced in the photoinduced reactions due to gauge invariance [31,32,40]. As a result, the contribution from the nucleon Born term to the $\gamma p \to K\Sigma$ reactions in our model is larger than the t-channel meson exchange. The Born term gives an important contribution to the S_{I1} waves in the $K^+\Sigma^0$ channel and to the S_{I1}, P_{I1}, and P_{I3} waves in the $K^0\Sigma^+$ channel, as shown in the right panels of Fig. 11. The contribution from the Born term to the angular distributions are also shown in Figs. 12 and 13. It is a challenge to explain the recent $K\Sigma$ photoproduction data with the small total cross section of the $\gamma p \to K^0\Sigma^+$ channel as compared to the $\gamma p \to K^+\Sigma^0$ reaction. We find that the initial input of t- and u-channel background and s-channel resonance contributions interfere in the final T matrix destructively, leading to the smaller total cross section for the $K^0\Sigma^+$ channel, while it is constructive in $K^+\Sigma^0$ channel. This difference is essential to suppress the total cross section of the $\gamma p \to K^0\Sigma^+$ channel in our present model. Though the agreement to the CLAS and CBELSA data is still poor as depicted in Fig. 11, it is clear that the data of the $K^0\Sigma^+$ channel provides an additional constraint for the model parameters. As a result, the extracted coupling at the $NK\Sigma$ vertex changes its sign compared to the previous Giessen model, as shown in Table III.

Since the background contribution, rescattering, and interference strongly influence the $\gamma p \to K\Sigma$ reactions, it is difficult to identify unambiguously individual resonance contributions only from the partial wave decomposition in Fig. 11. In order to give an overall understanding of the
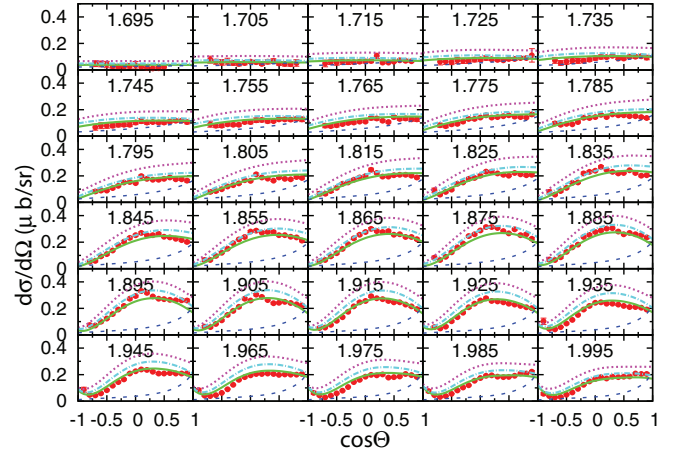
production mechanism, we demonstrate the rating of the resonances in the $K\Sigma$ photoproduction in the last column of Tables I and II, based on our present calculations. Here the rank is defined by the absolute variant value of the χ^2 in the $\gamma p \to K\Sigma$ reactions after turning off the corresponding resonance. So the highest ranking three stars ($\Delta\chi^2 > 10$) represent the significant role of these resonances, and two stars ($10 > \Delta\chi^2 > 5$) stand for a moderate contribution from the corresponding resonances. The one-star states ($\Delta\chi^2 < 5$) play only a minor or no role in the $\gamma p \to K\Sigma$ reactions. As can be seen from the ranking, in the isospin $I = 3/2$ sector the $P_{31}(1750)$, $P_{33}(1600)$, $D_{33}(1700)$, $D_{35}(1930)$, and $F_{35}(1905)$ resonances contribute most noticeably to the $K\Sigma$ photoproduction. In the isospin $I = 1/2$ sector, the contributions of the $S_{11}(1650)$, $P_{11}(1440)$, $D_{13}(1520)$, $D_{15}(1675)$, and $F_{15}(1680)$ states are most significant.

The $S_{11}(1650)$ state plays an important role in the S_{11} partial wave in both production channels at low energies. Close to threshold, the interference between $S_{11}(1650)$ and background develops a steep rise of the total cross section in the $K^0\Sigma^+$ channel as seen in Fig. 11. The kink structure around 1.72 GeV in the S_{11} partial wave is due to the ωN production threshold. The $S_{31}(1620)$ state plays an important role in the S_{31} partial wave which is, however, much smaller than the S_{11} channel. These two resonances, $S_{11}(1650)$ and $S_{31}(1620)$, have an obvious influence in the angular distributions of both channels, as shown in Figs. 12 and 13.

In the $K^+\Sigma^0$ channel, the $P_{31}(1750)$ resonance is important for producing a broad shoulder in the total cross sections around 1.8 GeV; see the lower panels of Fig. 11. In the $K^0\Sigma^+$ channel, $P_{31}(1750)$ is important not only for the peak around 1.8 GeV but also for the steep rise at high energies. A closer inspection reveals that these contributions overestimate the total cross sections in both the channels below 1.85 GeV, as can be seen in Fig. 11. In the $K^+\Sigma^0$ channel, $P_{31}(1750)$
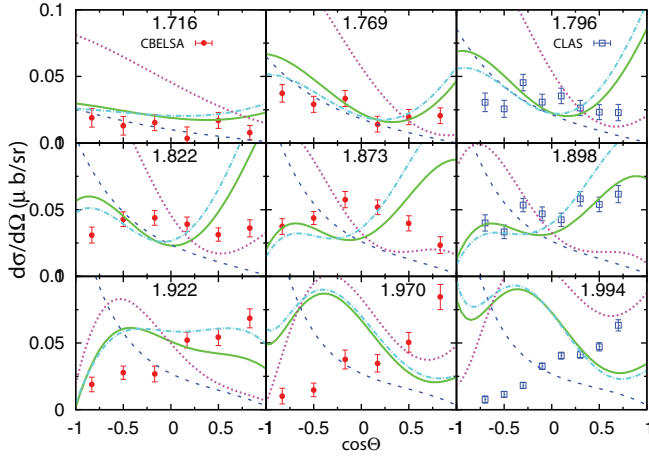
FIG. 13. (Color online) The differential cross section of the $\gamma p \to K^0 \Sigma^+$ reaction. The solid (green), dashed (blue), dotted (magenta), and dash-dotted (cyan) lines are the full model calculation, the contribution of the Born terms, and the model calculations with $S_{11}(1650)$ and $S_{31}(1620)$ turned off, respectively. The data are taken from CLAS [4] and CBELSA [10]. The numeric values label the center-of-mass energies in units of GeV.

contributes to the nonsymmetric shape of the beam asymmetry up to 1.85 GeV and the bump around 1.85 GeV in the backward angles in the recoil polarization; see Figs. 14 and 15 respectively. It also reduces considerably the magnitude of the double polarization C_z to the observed value in Fig. 16. In the recoil polarization of the $K^0 \Sigma^+$ channel, its effect can be seen but on a relatively low level.

The $D_{33}(1700)$ state is important for the shape of the beam asymmetry and recoil polarization in the $K^+ \Sigma^0$ channel. However, it shifts C_x to positive values, which seems to be unfavored by data, as shown in the left panels of Fig. 16. Other resonances, i.e., $P_{33}(1600)$, $P_{33}(1920)$, and $S_{31}(1900)$,
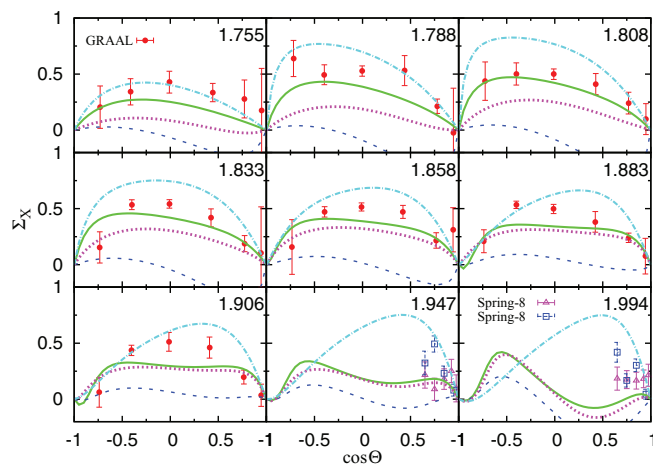

FIG. 14. (Color online) The beam asymmetry of $\gamma p \to K^+ \Sigma^0$ reaction. The solid (green), dashed (blue), dotted (magenta), and dash-dotted (cyan) lines are the full model calculation and the model calculations with $P_{31}(1750)$, $D_{33}(1700)$, and $D_{35}(1930)$ turned off, respectively. The data are taken from GRAAL [12] and LEPS [1–3]. The numeric values label the center-of-mass energies in units of GeV.

are important to bring the calculated C_x back to the negative values as demanded by the CLAS data.

Similar to the $\pi N \to K \Sigma$ reactions, the $D_{15}(1675)$ and $D_{35}(1930)$ resonances are clearly reflected in all observables in $K \Sigma$ photoproduction, as illustrated in Figs. 17 and 14. As shown in Fig. 14, $D_{35}(1930)$ is responsible for the backward peak in the beam asymmetry of the $K^+ \Sigma^0$ channel. The $F_{15}(1680)$ resonance is important for producing the backward structures in the angular distributions and polarization observables of both channels, as shown in Fig. 15.

The angular distribution of the $K^+ \Sigma^0$ channel in Fig. 12, showing a remarkable enhancement at forward angles, is induced by many resonances. Although the shape originates mainly from the $P_{31}(1750)$, $D_{13}(1520)$, $D_{33}(1700)$, and $D_{35}(1930)$ resonances, the contributions from $S_{11}(1650)$, $P_{33}(1600)$, and $D_{15}(1675)$ are also very important for reproducing the total magnitude. At high energies, two higher lying resonances $P_{13}(1900)$ and $F_{35}(1905)$ participate. The shape of the angular distribution is a result of the interference of these resonances with the background amplitudes. These resonances are equally important also for the beam asymmetry and polarization observables of the $K^+ \Sigma^0$ channel. The beam asymmetry and recoil polarization in Figs. 14, 12, and 17 are nicely reproduced. The calculated spin transfer coefficient C_x seems to be around zero but the CLAS data in the right panels of Fig. 16 indicate an increased negative value, so the fit quality of this observable needs improvement. As shown in the right panels of Fig. 16, the value of C_z is close to 1 and is trivially explained in our model, because it is mainly determined by the Born term with additional small structures from resonances.

As pointed out above, the broad peak in the $K^+ \Sigma^0$ differential cross sections, see Fig. 12, is produced by the interference of several resonances with background contributions. In the $K^0 \Sigma^+$ differential cross sections, where no obvious peak structure is observed in Fig. 13, the role of resonances and the background contributions still should be important. However, as seen in Fig. 13, the measured angular distributions are rather poorly described, becoming worse above 1.9 GeV. As shown in the upper right panels of Fig. 11, at high energies the P_{I1} partial wave from the background is contributing significantly to this channel. But the contribution of resonances is not enough to provide a destructive interference to compensate this P_{I1}-wave excess, which results in a poor description of both total and differential cross sections at high energies. In contrast, the recoil polarization data in Fig. 17 seem to be structureless and flat within the experimental errors.

In the $\pi N \to K \Sigma$ reactions, it has been shown that the data of angular distributions and polarization observables provide plenty of information on the individual partial waves. This effect is seen clearly in $K \Sigma$ photoproduction. Among the lowest rank states, the $P_{11}(1710)$, $F_{15}(2000)$, and $F_{35}(2000)$ have visible effects on the magnitude of the total and differential cross sections of the $K^0 \Sigma^+$ channel. Though $F_{35}(1905)$ hardly affects the total cross sections, it influences considerably the double polarization observables of $K^+ \Sigma^0$ channel at high energies; for an illustration see Fig. 16. The one-star states in our ranking, the $P_{33}(1232)$ and $P_{33}(1920)$ resonances, are seen in the angular distributions and polarization observables of both channels. The $D_{13}(1950)$ state seems to be of minor
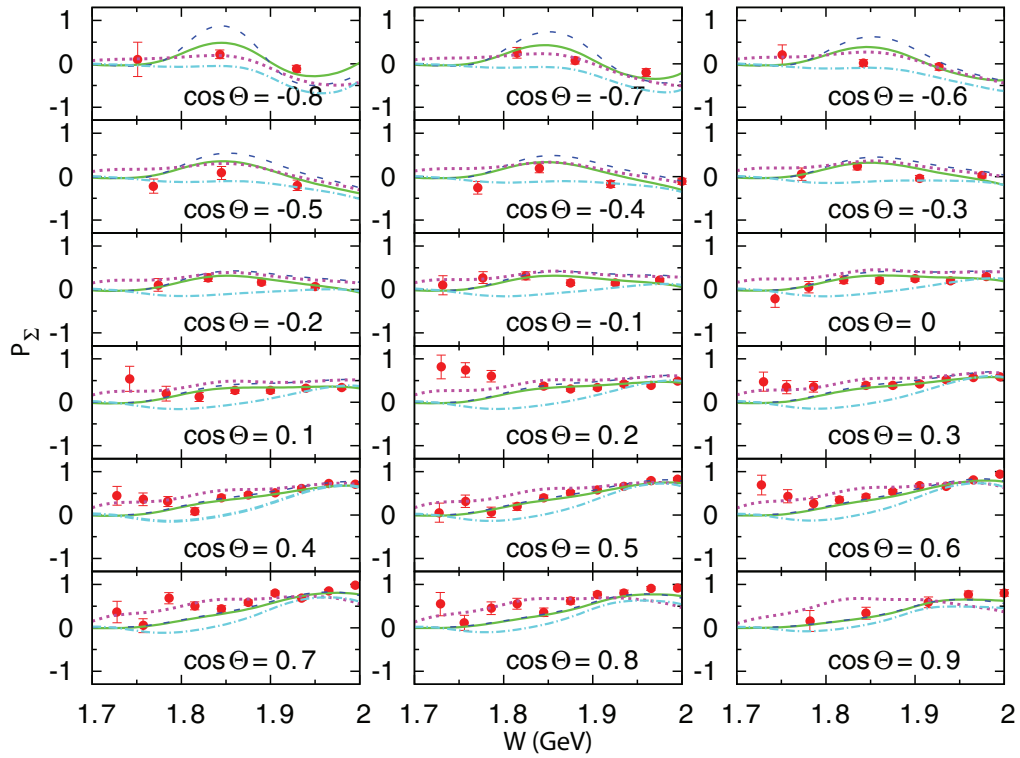
FIG. 15. (Color online) The recoil polarization of $\gamma p \to K^+\Sigma^0$ reaction. The solid (green), dotted (magenta), dash-dotted (cyan), and dashed (blue) lines are the full model calculation and the model calculations with $P_{31}(1750)$, $D_{33}(1700)$, and $F_{15}(1680)$ turned off, respectively. The data are taken from CLAS [8].

importance and it is the only resonance that is hardly seen in all observables.

D. Discussion

From the present analysis of the new $K\Sigma$ photoproduction data we have obtained stringent constraints on the resonance

couplings in our Lagrangian. The values of the coupling constants for the strangeness-carrying vertices derived here are compared to the previously obtained results [30] in Table III. The least change is found in the $NK_0^*\Sigma$ couplings, which in magnitude are increased by about 20%. The $NK\Sigma$ coupling constants are altered more drastically: besides a change of
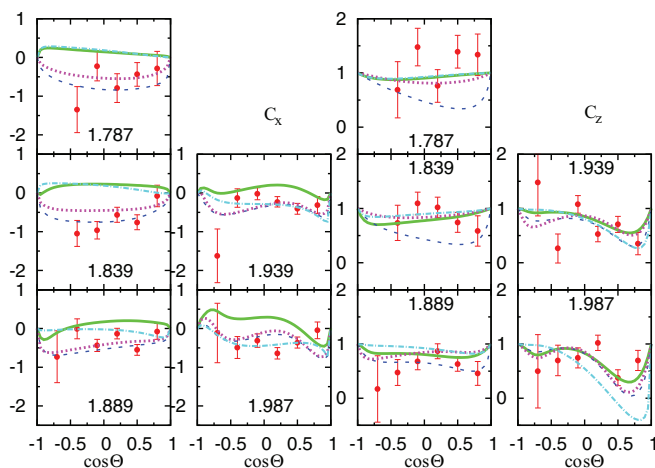

FIG. 16. (Color online) The spin transfer coefficients C_x and C_z in the $\gamma p \to K^+\Sigma^0$ reaction. The solid (green), dashed (blue), dotted (magenta), and dash-dotted (cyan) lines are the full model calculation and the model calculations with $P_{31}(1750)$, $D_{33}(1700)$, and $F_{35}(1905)$ turned off, respectively. The data are taken from CLAS [7]. The numeric values label the center-of-mass energies in units of GeV.
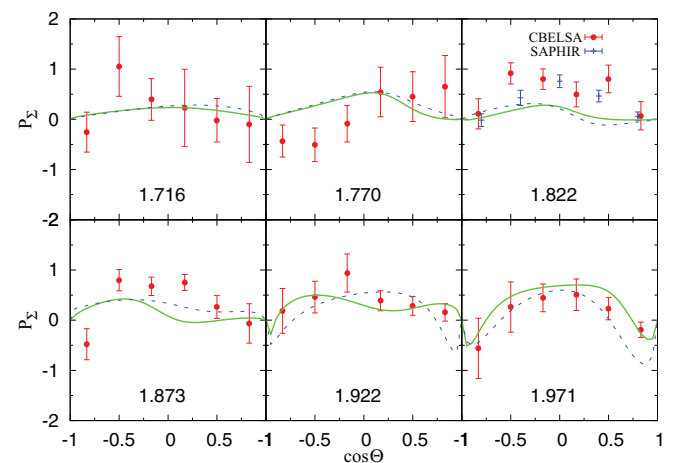

FIG. 17. (Color online) The recoil polarization of the $\gamma p \to K^0\Sigma^+$ reaction. The solid (green) and dashed (blue) lines are the full model calculation and the model calculation with $D_{15}(1675)$ turned off, respectively. The data are taken from CBELSA [10] and SAPHIR [14]. The SAPHIR data is only for comparison and is not used in the parameters' fitting. The numeric values label the center-of-mass energies in units of GeV.

sign their magnitude is increased by a factor of more than 2. This sign change is important because it leads the small total cross sections of the $\gamma p \rightarrow K^0 \Sigma^+$ channel, as pointed out in Sec. III C. There is always an ambiguity in the sign of different couplings constants; for example the definition of $NK\Sigma$ coupling in Ref. [41] differs from ours in sign. However, in SU(3) symmetry the relative sign of $NK\Sigma$ and $NK\Lambda$ is negative [20]. The $NK\Lambda$ coupling extracted earlier [37] is of the same sign as the present $NK\Sigma$ coupling, indicating that our analysis does not follow the SU(3) relations. A similar result was found also in the Usov and Scholten approach [40,41] as well as in other models [20]. It should be noted that our negative $NK\Lambda$ coupling is extracted from data published before 2007, so it is interesting to check this sign problem after including the enlarged polarization data on $K\Lambda$ photoproduction into the analysis. Also, the $NK^*\Sigma$ and $NK_1\Sigma$ coupling constants are significantly modified: we obtain much smaller values than in [30]. As a result, the contributions of the t-channel K^* and K_1 meson exchange are decreased, while the strength of the K_0^* part is slightly increased.

The couplings of some resonances to the $K\Sigma$ channel are very small, even approaching zero, but this does not mean that they have no influence in the $K\Sigma$ production. They still can contribute through coupled-channel and interference effects. That, in fact, is an important reason why the model demands many resonances, but only few of them, i.e., the $D_{13}(1520)$, $D_{15}(1675)$, $D_{35}(1930)$, and $F_{15}(1680)$ states, have large couplings to the $K\Sigma$ final channel. As seen in Table I, the coupling constant of $P_{11}(1710)$ to the $K\Sigma$ channel is much smaller than in the previous Giessen analysis, so its contribution is suppressed. In the isospin $I = 3/2$ sector, the sign of the coupling constants of the $S_{31}(1620)$ and $P_{33}(1600)$ resonances to the $K\Sigma$ channel is opposite to those of the previous Giessen model, as can be seen in Table II. Also the electromagnetic helicity amplitudes of the $P_{31}(1750)$ state are much smaller than in the previous investigations (see Table II). Hence, the contribution of this state to $K\Sigma$ photoproduction is decreased compared to our previous analysis. This effect is more pronounced at high energies.

In the Bonn-Gatchina partial wave analysis, the $S_{11}(1535)$, $S_{11}(1650)$, $P_{13}(1720)$, and $P_{11}(1840)$ states give the main contributions to hyperon photoproduction [25]. Especially the C_x and C_z observables in the $K^+\Sigma^0$ channel require an additional $P_{13}(1900)$ resonance, as stressed in their analysis [24]. In our model, however, we include this resonance into the formulation from the very beginning [30,31] and in this paper we confirm its importance in $K\Sigma$ photoproduction, especially at high energies. In a covariant isobar model [57] this resonance is also found to be important in producing the cross section peak around 1.9 GeV in $\gamma p \rightarrow K^+\Lambda$. However, in the Giessen model this peak is caused by the interference effect of P_{13} resonance and background terms [37]. In the Bonn-Gatchina model, a high lying P_{11} state with a mass of 1840 MeV is found to be important for $K\Sigma$ photoproduction, and a third S_{11} state with the mass around 1900 MeV is also needed in the global fit, though only weakly contributing to $K\Sigma$ photoproduction. In order to check that conclusion we had added separately and arbitrarily an S_{11}, an S_{31}, a P_{11}, and a P_{31} resonance with BW masses varying from 1700 to 2000 MeV

to our model, but without finding any evidence for such a contribution.

A puzzling result is the difference in the description of the $K^0\Sigma^+$ and the $K^+\Sigma^0$ photoproduction data. At practically all energies the $K^+\Sigma^0$ data are well described, including angular distributions of cross sections and polarization observables. In the complementary channel $K^0\Sigma^+$ that we achieve, however, the measured observables are considerably less accurately reproduced; e.g., Fig. 13. The differences are showing up most clearly in the differential observables, indicating remaining uncertainties in phase relations, obviously affecting the resulting interference pattern. Taking the valence quark configuration as a guideline, the two channels differ only by the final distribution of u and d quarks among the two hadrons: the reaction $\gamma p \rightarrow K^0\Sigma^+$ corresponds to $K^0(d\bar{s}) + \Sigma^+(uus)$ while the reaction $\gamma p \rightarrow K^+\Sigma^0$ is leading to $K^+(u\bar{s}) + \Sigma^0(uds)$. Assuming charge symmetry at the quark (and hadron) level, the two-channel configurations should behave perfectly the same, except for particular threshold contributions or resonances coupling differently to the two exit channels.

In our model the driving force for the population of the $K^0\Sigma^+$ channel is the nucleon-photon Born term, while in the Bonn-Gatchina model the main contribution is the t-channel K meson exchange [25]. It should be mentioned that their agreement with $K^0\Sigma^+$ data is worse than that for the $K^+\Sigma^0$ channel, and their fit of C_x leads to a χ^2 value of little less than 3.0, larger than that of C_z [23]. These findings are in line with the results of our model so it seems that the $\gamma p \rightarrow K^0\Sigma^+$ reaction really needs further study in the future.

The recent analysis performed by Shyam *et al.* [41] within the Usov and Scholten model [40] obtains a good description of the SAPHIR data but not the CLAS data. In that analysis the $\gamma p \rightarrow K^+\Sigma^0$ reaction is dominated by the background and the $P_{33}(1600)$ resonance predicting a much simpler production mechanism. It should be pointed out that in Ref. [41] the $\gamma p \rightarrow K^0\Sigma^+$ channel, which poses strong constraints to the model parameters in our extended approach, was not included in the analysis.

IV. SUMMARY

In the present paper, we perform a coupled-channel analysis which uses effective Lagrangian and respects unitary and gauge invariance to the $(\pi, \gamma)N \rightarrow K\Sigma$ reactions up to a center-of-mass energy of 2.0 GeV. The available data of pion- and photon-induced reactions are simultaneously analyzed to investigate the reaction mechanism. The meson-baryon coupling constants and resonance couplings to the $K\Sigma$ state are extracted. Several resonances contribute to the process. The coherent sum of resonances and background contributions is essential to describe the recent photoproduction data obtained by the CLAS, CBELSA, LEPS, and GRAAL groups. It has been shown that the $K\Sigma$ production mechanism is much more complicated than that concluded from the previous Giessen model studies after taking into account these new data. Overall, our results agree well with the data. However, there are puzzling exceptions, namely the double polarization spin transfer coefficients in $\gamma p \rightarrow K^+\Sigma^0$ and the differential cross sections

of $\gamma p \to K^0 \Sigma^+$, which are awaiting further investigation. In our planned model improvements and reformulations, one of the crucial directions is to treat the $2\pi N$ channels as the real ρN, $\pi\Delta$, and σN states, which is under progress and will be the topic of separate publications. On the other hand, extrapolations into the complex plane and extracting the poles and residues of the full amplitudes are of fundamental interest and should be considered as a major direction in the future. In summary, we find that $K\Sigma$ production is a good probe to explore the isospin $I = 3/2$ resonances. Our results are shedding light on the search for missing resonances and the $K\Sigma$ production mechanism in other reactions; for example,

the long-standing controversy in the close-to-threshold behavior of the $pp \to nK^+\Sigma^+$ reaction [58].

[1] R. G. T. Zegers *et al.* (LEPS Collaboration), Phys. Rev. Lett. **91**, 092001 (2003).

[2] M. Sumihama *et al.* (LEPS Collaboration), Phys. Rev. C **73**, 035214 (2006).

[3] H. Kohri *et al.* (LEPS Collaboration), Phys. Rev. Lett. **97**, 082003 (2006).

[4] B. Carnahan, Ph.D. thesis, The Catholic University of America, 2003 (unpublished).

[5] J. W. C. McNabb *et al.* (CLAS Collaboration), Phys. Rev. C **69**, 042201(R) (2004); J. W. C. McNabb, Ph.D. thesis, Carnegie Mellon University, 2002 (unpublished).

[6] R. Bradford *et al.* (CLAS Collaboration), Phys. Rev. C **73**, 035202 (2006).

[7] R. K. Bradford *et al.* (CLAS Collaboration), Phys. Rev. C **75**, 035205 (2007).

[8] B. Dey *et al.* (CLAS Collaboration), Phys. Rev. C **82**, 025202 (2010).

[9] S. Anefalos Pereira *et al.* (CLAS Collaboration), Phys. Lett. B **688**, 289 (2010).

[10] R. Castelijns *et al.* (CBELSA/TAPS Collaboration), Eur. Phys. J. A **35**, 39 (2008).

[11] R. Ewald *et al.* (CBELSA/TAPS Collaboration), Phys. Lett. B **713**, 180 (2012).

[12] A. Lleres *et al.* (GRAAL-ESRF Collaboration), Eur. Phys. J. A **31**, 79 (2007).

[13] K. H. Glander *et al.* (SAPHIR Collaboration), Eur. Phys. J. A **19**, 251 (2004).

[14] R. Lawall *et al.* (SAPHIR Collaboration), Eur. Phys. J. A **24**, 275 (2005).

[15] D. S. Carman *et al.* (CLAS Collaboration), Phys. Rev. C **79**, 065205 (2009).

[16] P. Achenbach *et al.* (A1 Collaboration), Eur. Phys. J. A **48**, 14 (2012).

[17] T. Mart, C. Bennhold, and C. E. Hyde-Wright, Phys. Rev. C **51**, R1074 (1995).

[18] T. Mart, Phys. Rev. C **62**, 038201 (2000).

[19] S. Janssen, J. Ryckebusch, D. Debruyne, and T. Van Cauteren, Phys. Rev. C **66**, 035202 (2002).

[20] J. C. David, C. Fayard, G. H. Lamot, and B. Saghai, Phys. Rev. C **53**, 2613 (1996).

[21] Z. Li, Phys. Rev. C **52**, 1648 (1995); Z. Li, W.-H. Ma, and L. Zhang, *ibid.* **54**, R2171 (1996).

[22] A. V. Anisovich, R. Beck, E. Klempt *et al.*, Eur. Phys. J. A **48**, 15 (2012).

[23] A. V. Anisovich, E. Klempt, V. A. Nikonov *et al.*, Eur. Phys. J. A **47**, 27 (2011).

[24] V. A. Nikonov, A. V. Anisovich, E. Klempt *et al.*, Phys. Lett. B **662**, 245 (2008).

[25] A. V. Anisovich, V. Kleber, E. Klempt *et al.*, Eur. Phys. J. A **34**, 243 (2007).

[26] A. V. Sarantsev, V. A. Nikonov, A. V. Anisovich *et al.*, Eur. Phys. J. A **25**, 441 (2005).

[27] A. V. Anisovich, E. Klempt, A. V. Sarantsev *et al.*, Eur. Phys. J. A **24**, 111 (2005).

[28] T. Feuster and U. Mosel, Phys. Rev. C **58**, 457 (1998).

[29] T. Feuster and U. Mosel, Phys. Rev. C **59**, 460 (1999).

[30] G. Penner and U. Mosel, Phys. Rev. C **66**, 055211 (2002).

[31] G. Penner and U. Mosel, Phys. Rev. C **66**, 055212 (2002).

[32] G. Penner, Ph.D. thesis (in English), Universität Giessen, 2002 (unpublished), available via http://theorie.physik.uni-giessen.de.

[33] V. Shklyar, G. Penner, and U. Mosel, Eur. Phys. J. A **21**, 445 (2004).

[34] V. Shklyar, H. Lenske, U. Mosel, and G. Penner, Phys. Rev. C **71**, 055206 (2005).

[35] V. Shklyar, H. Lenske, and U. Mosel, Phys. Lett. B **650**, 172 (2007).

[36] V. Shklyar, H. Lenske, and U. Mosel, Phys. Rev. C **87**, 015201 (2013).

[37] V. Shklyar, H. Lenske, and U. Mosel, Phys. Rev. C **72**, 015210 (2005).

[38] T. Mart and C. Bennhold, Phys. Rev. C **61**, 012201(R) (1999).

[39] T. Corthals, T. Van Cauteren, J. Ryckebusch, and D. G. Ireland, Phys. Rev. C **75**, 045204 (2007).

[40] A. Usov and O. Scholten, Phys. Rev. C **72**, 025205 (2005).

[41] R. Shyam, O. Scholten, and H. Lenske, Phys. Rev. C **81**, 015204 (2010).

[42] M. Döring, C. Hanhart, F. Huang *et al.*, Nucl. Phys. A **851**, 58 (2011).

[43] D. Rönchen, M. Döring, F. Huang *et al.*, Eur. Phys. J. A **49**, 44 (2013).

[44] F. Huang, M. Döring, H. Haberzettl *et al.*, Phys. Rev. C **85**, 054003 (2012).

[45] B. Juliá-Díaz, B. Saghai, T.-S. H. Lee, and F. Tabakin, Phys. Rev. C **73**, 055204 (2006).

[46] B. Borasoy, P. C. Bruns, U.-G. Meissner *et al.*, Eur. Phys. J. A **34**, 161 (2007).

[47] K. Nakamura (Particle Data Group), J. Phys. G **37**, 075021 (2010).

[48] D. M. Manley and E. M. Saleski, Phys. Rev. D **45**, 4002 (1992).

[49] M. Shrestha and D. M. Manley, Phys. Rev. C **86**, 055203 (2012).

[50] T. P. Vrana, S. A. Dytman, and T.-S. H. Lee, Phys. Rep. **328**, 181 (2000).

[51] R. A. Arndt, I. I. Strakovsky, R. L. Workman, and M. M. Pavan, Phys. Rev. C **52**, 2120 (1995); R. A. Arndt, I. I. Strakovsky, and R. L. Workman, *ibid*. **53**, 430 (1996).

[52] R. A. Arndt, W. J. Briscoe, I. I. Strakovsky, R. L. Workman, and M. M. Pavan, Phys. Rev. C **69**, 035213 (2004).

[53] D. M. Manley, R. A. Arndt, Y. Goradia, and V. L. Teplitz, Phys. Rev. D **30**, 904 (1984).

[54] R. A. Arndt, W. J. Briscoe, I. I. Strakovsky, and R. L. Workman, Phys. Rev. C **66**, 055213 (2002).

[55] R. L. Workman, W. J. Briscoe, M. W. Paris, and I. I. Strakovsky, Phys. Rev. C **85**, 025201 (2012).

[56] X. Cao, B.-S. Zou, and H.-S. Xu, Phys. Rev. C **81**, 065201 (2010); Nucl. Phys. A **861**, 23 (2011); Int. J. Mod. Phys. A **26**, 505 (2011).

[57] T. Mart and M. J. Kholili, Phys. Rev. C **86**, 022201(R) (2012).

[58] X. Cao, X.-G. Lee, and Q.-W. Wang, Chin. Phys. Lett. **25**, 888 (2008); J.-J. Xie and B.-S. Zou, Phys. Lett. B **649**, 405 (2007).